Qian Zhang, Wenchun Jiang* and Yanting Zhang

Effect of geometrical parameters on the effective elastic modulus for an X-type lattice truss panel structure

https://doi.org/10.1515/secm-2017-0257 Received July 28, 2017; accepted October 24, 2017; previously published online January 17, 2018

Abstract: The lattice truss panel structure (LTPS), which is a high strength material with high efficiency of heat transfer, has a good potential to be used as compact heat exchanger. The core of LTPS is a periodic porous structure, and the effective elastic modulus (EEM) will be different from the base material. It is essential to calculate the EEM for the design of this type of heat exchanger. This paper presents a study on the EEM of X-type LTPS by homogenization method, which has been verified by finite element method (FEM). It reveals that the effects of seven geometrical parameters of the X-type LTPS on EEM are not identical, and the relationship between the seven parameters and EEM has been established. Results calculated by homogenization method and FEM show a good agreement. The EEM decreases with the increase of truss length, stamping angle, shearing angle and node length, while it increases with the increase of truss width, truss thickness and face sheet thickness. Unlike the conventional foam material, there is no clear correlation between the EEM and the relative density, and a formula has been fitted to calculate the EEM of LTPS.

Keywords: effective elastic modulus; finite element method; homogenization method; lattice truss panel structure.

1 Introduction

Lattice truss panel structures (LTPS) are widely used in aerospace and astronautic engineering aspect because of the

*Corresponding author: Wenchun Jiang, State Key Laboratory of Heavy Oil Processing, College of Chemical Engineering, China University of Petroleum (East China), Qingdao, 266580, P.R. China, Phone: +86 532 86980609, Fax: +86 532 86980609,

e-mail: jiangwenchun@126.com

Qian Zhang: College of Mechanical and Electronic Engineering, China University of Petroleum (East China), Qingdao, 266580, P.R. China; and State Key Laboratory of Heavy Oil Processing, College of Chemical Engineering, China University of Petroleum (East China), Qingdao, 266580, P.R. China

Yanting Zhang: College of Mechanical and Electronic Engineering, China University of Petroleum (East China), Qingdao, 266580, P.R. China low density and high strength [1]. In addition, LTPS are also a highly efficient heat exchanger because of the low thermal resistance, large surface contact area between the core and a coolant, high heat transfer between the metal surface and the fluid, vortex structures formed behind the vertices and flow separation on the truss surfaces [2, 3]. The LTPS made of high temperature resistance material has a good potential to be used at high temperatures because of the high strength, for example as cooling systems of modern steam turbine [4]. These heat exchangers, which operate at high temperature or fatigue conditions, are required to have high strength and reliability. The core of LTPS is a kind of periodic porous structure, and its effective mechanical strength will be different from the parent material. How to calculate the effective mechanical strength of LTPS is critical for the design of this heat exchanger. In the past 10 years, many researchers have carried out extensive work on the fabrication technology [5-7], mechanical strength [8-10] and effective elastic modulus (EEM) of LTPS [11, 12]. In this paper, the main focus is on the EEM of LTPS, and thus the following literature review is mainly on the EEM.

Extensive work has been paid on the EEM of foam or cellular materials in the past decades. Early in the 1980s, Torquato et al. [13] developed an analytical model to predict the EEM of honeycomb structure, assuming that the linear elastic behavior is controlled by the bending of cell wall. The EEM is a function of relative density relating to wall length and thickness, and it does not depend on the Poisson's ratio of the solid phase. Basing on this theory, in the 2000s, Wallach and Gibson [14] studied the EEM of a threedimensional truss material as a function of the aspect ratio of the unit cell, and the results have a good agreement with the experimental data. For the foam material, it is very difficult to get an analytical model because the geometrical structure is more complex than the honeycomb structure. Thus, finite element method (FEM) has been widely used to predict the EEM. For instance, Sanders and Gibson [15] used FEM to study the EEM of hollow sphere foams and found that the hollow sphere foams have the potential for improved mechanical properties compared with existing metallic foams, and the EEM of face-centered cubic packing of hollow sphere foams is larger than those of body-centered cubic and simple cubic packing [16]. Guessasma et al. [17] investigated the relation of the cellular structure to Young's

modulus of open cell materials by FEM; they found that the Young's modulus is a function of relative density for different sphere distribution widths and overlap distances. Guessasma [18] found an exponential correlation between the EEM and relative density for a 2D cellular structure by FEM study. In recent years, Antunes et al. [19] and Marur [20] used FEM to study the EEM of syntactic foams. And the influence of the matrix, reinforcement, the radius and thickness of hollow particles, and the volume fraction of particles on the EEM of syntactic foams have been fully studied. Pérez et al. [21, 22] found that the EEM drops as the porosity increases for Mg and Ti foams by FEM study. Liu and Antoniou [23] built a relationship between the EEM and geometrical structure of a nanoporous metal foam. Chen et al. [24] studied the EEM of a porous $La_{0.6}Sr_{0.4}Co_{0.2}Fe_{0.8}O_{3-\delta}$ ceramic film by FEM based on the reconstructed microstructures, and they found that in the initial stages of sintering, when interparticle necks are small, the EEM increases with neck size increase. However, as the coarsening increases further, the EEM becomes insensitive to the details of the microstructure and only depends on porosity.

LTPS composed of two face sheets and the lattice truss core is a more complex structure than the foam and honeycomb structures. But the core is a periodic structure, and the homogenization method becomes an effective method to characterize the mechanical behavior [25]. Liu et al. [26, 27] studied the EEM and performed the design optimization of truss-cored sandwiches by homogenization method. Zhang et al. [28] reported a new type of lattice structure named X-type LTPS whose out of plane compressive and shear peak strength are about 30% larger than pyramidal LTPS with the same relative density. Besides, Zhang et al. [29] used homogenization method to study the effective elastic constants of an X-type LTPS, and the obtained results agree well with the data by experimental method and FEM. But the relationship between geometrical parameters and the EEM has not been established. In this paper, the EEM of X-type LTPS has been investigated by homogenization method and FEM; meanwhile, the influence of the seven geometric parameters on the EEM of X-type LTPS is explored. Basing on the comprehensive study, a formula has been fitted to calculate the EEM considering all the geometrical parameters.

2 Homogenization method

2.1 Homogenization theory

The X-type LTPS consists of upper face sheet, lower face sheet, and a truss core, as shown in Figure 1. The basic

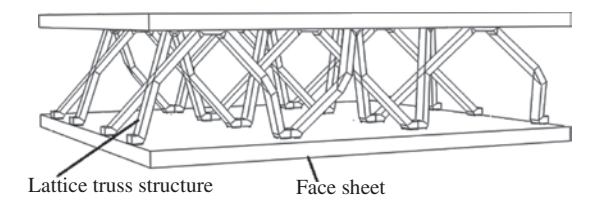


Figure 1: Schematic of X-type lattice truss panel structure.

material used in this work is P92 steel, and its elastic modulus and Poisson's ratio are 203 GPa and 0.3, respectively. The X-type LTPS is a kind of periodic cellular structure whose mechanical properties can be analyzed by a representative unit cell, as shown in Figure 2. The geometrical parameters of X-type LTPS: the truss length L, truss width w, truss thickness t, face sheet thickness T, node length *S*, stamping angle α and shearing angle β are listed in Table 1. The length L_v , width L_v and height H of the unit cell are 21, 28 and 14 mm, respectively.

According to homogenization method, the X-type LTPS is deemed as a homogeneous solid at the macroscopic scale, while it is considered as discrete structural elements at microscopic scale [26]. Considering the continuum mechanics and homogenized theory, the relationship between macroscopic scale and microscopic scale for strain and stress can be described as

$$\Xi = \langle \varepsilon \rangle_{\Omega} \equiv \frac{1}{\Omega} \int_{\Omega} \varepsilon d\Omega \tag{1}$$

$$\Sigma = \langle \sigma \rangle_{\Omega} \equiv \frac{1}{\Omega} \int_{\Omega} \sigma d\Omega$$
 (2)

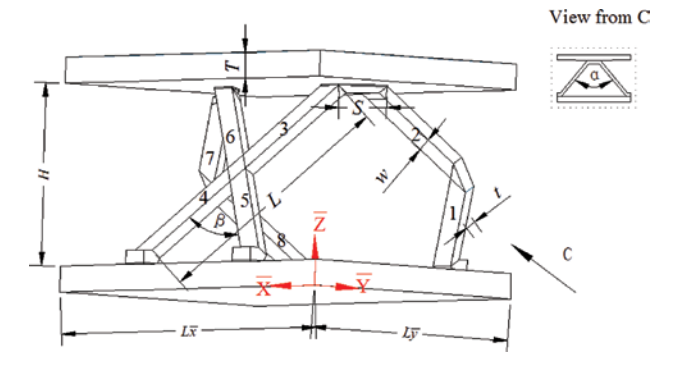


Figure 2: Sketching of the unit cell.

Table 1: Geometrical parameters of X-type LTPS.

L	W	t	T	S	α	β
22 mm	2 mm	1 mm	2 mm	3 mm	60°	70°

the volume of the unit cell.

The volume averaged strain energy density of an inhomogeneous material is determined by multiplying the separate volume averages of microscopic stresses and strains [26]:

$$\Sigma \cdot \Xi = \langle \sigma \cdot \varepsilon \rangle_{\Omega} = \frac{1}{\Omega} \int_{\Omega} \sigma \cdot \varepsilon d\Omega$$
 (3)

where $\Sigma \cdot \Xi$ is the macroscopic strain energy density and $\int_\Omega \sigma \cdot \varepsilon d\Omega$ is the total strain energy of the admissible microscopic field.

Eight beams of the unit cell would be analyzed to study the mechanical properties of the X-type LTPS. According to the deformation analysis of the unit cell, the displacements of the end nodes of the beam are

$$\Delta = L_0 \Xi n_0 \tag{4}$$

where Ξ is the three-order equivalent strain tensor, L_0 means the length of the beam, and n_0 denotes the direction vector of the beam in global coordinate system:

$$\Xi = \begin{bmatrix} \Xi_{11} & \Xi_{12} & \Xi_{13} \\ & \Xi_{22} & \Xi_{23} \\ \text{sym} & \Xi_{33} \end{bmatrix}$$
 (5)

$$n_0 = (n_1', n_2', n_3')^T$$
 (6)

$$\Delta = (\Delta_1, \, \Delta_2, \, \Delta_3)^T \tag{7}$$

Because each sub-geometry (the unit cell) of X-type LTPS contains equal truss members and the length of the trusses is equal. Then, using the Euler-Bernoulli beam model derived from mechanics of materials, the axial stretching of the beam prevails over the bending deformation [26]. Therefore, the bending deformation and associated rotations are neglected here. The nodal displacement vector $u^{(i)}$ for the ith beam can be characterized by the two ends of the beam. For $u^{(i)}$, The previous six values represent displacement of the one end, and the following six values denotes that of the other end:

$$u^{(i)} = [\Delta_1, \Delta_2, \Delta_3, \omega_1, \omega_2, \omega_3, 0, 0, 0, 0, 0, 0]^{(i)T}$$
 (8)

where the ω means the rotation:

$$[\omega_1, \omega_2, \omega_3]^T = 0 (9)$$

If the unit cell is composed of N Euler-Bernoulli beam members, its strain energy density can be defined as

$$U^* = \frac{1}{\Omega} \sum_{i=1}^{N} \frac{1}{2} u^{(i)T} K^{(i)} u^{(i)}$$
 (10)

where Ω is the volume of the unit cell, $u^{(i)}$ is the nodal displacement vector of the ith beam, and $K^{(i)}$ is the global stiffness matrix that satisfies the transformation between local and global coordinates; it can be calculated by

$$K^{(i)} = T'^{\mathsf{T}} K^{e(i)} T' \tag{11}$$

where T' is the transformation matrix, which is related with the global coordinate system and the local coordinate system of the beam element. $K^{e(i)}$ is the element stiffness matrix:

$$K^{e(i)} = \begin{bmatrix} k_1 & k_2 \\ \text{sym} & k_3 \end{bmatrix}^{e(i)}$$
 (12a)

$$k_{1} = \begin{bmatrix} \frac{EA}{l} & 0 & 0 & 0 & 0 & 0 \\ 0 & \frac{12EI_{z}}{l^{3}} & 0 & 0 & 0 & \frac{6EI_{z}}{l^{2}} \\ 0 & 0 & \frac{12EI_{y}}{l^{3}} & 0 & \frac{-6EI_{y}}{l^{2}} & 0 \\ 0 & 0 & 0 & \frac{GI_{x}}{l} & 0 & 0 \\ 0 & 0 & \frac{-6EI_{y}}{l^{2}} & 0 & \frac{4EI_{y}}{l} & 0 \\ 0 & \frac{6EI_{z}}{l^{2}} & 0 & 0 & 0 & \frac{4EI_{z}}{l} \end{bmatrix}$$
(12b)

$$k_{2} = \begin{bmatrix} -\frac{EA}{l} & 0 & 0 & 0 & 0 & 0\\ 0 & -\frac{12EI_{z}}{l^{3}} & 0 & 0 & 0 & \frac{6EI_{z}}{l^{2}} \\ 0 & 0 & \frac{12EI_{y}}{l^{3}} & 0 & \frac{-6EI_{y}}{l^{2}} & 0\\ 0 & 0 & 0 & \frac{GI_{x}}{l} & 0 & 0\\ 0 & 0 & \frac{6EI_{y}}{l^{2}} & 0 & \frac{2EI_{y}}{l} & 0\\ 0 & \frac{6EI_{z}}{l^{2}} & 0 & 0 & 0 & \frac{2EI_{z}}{l} \end{bmatrix}$$
(12c)

$$k_{3} = \begin{bmatrix} \frac{EA}{l} & 0 & 0 & 0 & 0 & 0\\ 0 & \frac{12EI_{z}}{l^{3}} & 0 & 0 & 0 & -\frac{6EI_{z}}{l^{2}} \\ 0 & 0 & \frac{12EI_{y}}{l^{3}} & 0 & \frac{6EI_{y}}{l^{2}} & 0\\ 0 & 0 & 0 & \frac{GI_{x}}{l} & 0 & 0\\ 0 & 0 & \frac{6EI_{y}}{l^{2}} & 0 & \frac{4EI_{y}}{l} & 0\\ 0 & \frac{-6EI_{z}}{l^{2}} & 0 & 0 & 0 & \frac{4EI_{z}}{l} \end{bmatrix}$$
(12d)

The macroscopic strain vector acting on the unit cell is defined as

$$\Gamma = \left[\Gamma_{11}, \Gamma_{22}, \Gamma_{33}, \Gamma_{23}, \Gamma_{13}, \Gamma_{12}\right]^{T}$$

$$= \left[\Xi_{11}, \Xi_{22}, \Xi_{33}, 2\Xi_{23}, 2\Xi_{13}, 2\Xi_{12}\right]^{T}$$
(13)

The effective stiffness of the unit cell can be calculated as [26]

$$C^{H}_{ijkl} = \frac{\partial^{2} U^{*}}{\partial \Gamma_{ij} \partial \Gamma_{kl}}$$
 (14)

where H denotes the homogenized effective stiffness.

Combining Equations (10) and (14), the effective stiffness matrix of the X-type LTPS is calculated by a program compiled by Matlab code:

$$C^{H} = \begin{cases} 67.62 & 219.5 & 220.2 & 0 & 0 & 0 \\ 219.5 & 865 & 764.9 & 0 & 0 & 0 \\ 220.2 & 764.9 & 782.6 & 0 & 0 & 0 \\ 0 & 0 & 0 & 793.9 & 0 & 0 \\ 0 & 0 & 0 & 0 & 225.1 & 0 \\ 0 & 0 & 0 & 0 & 0 & 230.7 \end{cases}$$
MPa (15)

It is obvious that the stiffness matrix has nine independent parameters, namely, C_{1111} , C_{1122} , C_{1133} , C_{2222} , C_{2233} , C_{3333} , C_{1212} , C_{1313} and C_{2323} , indicating that the core is regarded as an orthotropic material after the homogenization.

2.2 Calculation of the effective elastic modulus

The homogenous calculation in Section 2.1 just gets the effective stiffness matrix of the X-type core of LTPS. In order to calculate the EEM of the whole panel structure, a three-dimensional equivalent model is established by finite element software ABAQUS, as shown in Figure 3. The X-type core is assumed to be an equivalent homogenous-solid plate with the same length, width, and height

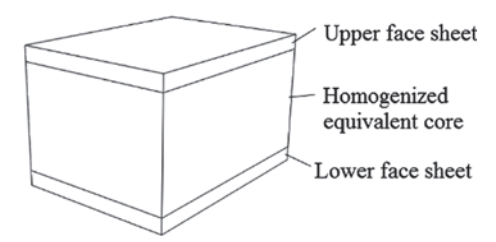


Figure 3: Equivalent homogenous solid plate model.

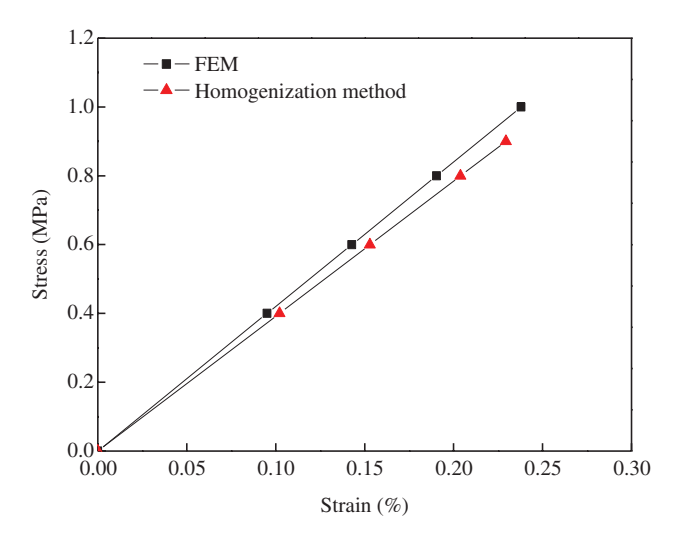


Figure 4: The elastic stage of the equivalent stress-strain curves by homogenization method and FEM.

of X-type core. The effective elastic constants of the equivalent homogenous-solid plate are specified by the effective stiffness matrix obtained in Section 2.1 (Equation (15)). The equivalent solid plate is bonded tightly to the upper face sheet and lower face sheet to form a sandwich panel with three layers.

A finite element analysis of the uniaxial tensile test was performed to calculate the EEM of the X-type core of LTPS. In order to get a uniform deformation of the model, a rigid plate was added and bonded tightly to the top surface of the upper face sheet. A tensile load was applied on the rigid plate, and the effective strain is calculated by the displacement of rigid plate divided by the original height of the composite plate. A plot of the obtained elastic stage of the equivalent stress-strain curve is shown in Figure 4, and the curve slope is the EEM.

3 Verification by finite element method

In order to verify the homogenization method, a solid three-dimensional finite element analysis was performed. And the analysis using FEM is carried out by using ABAQUS software. The materials of face sheets and trusses are P92 steel as before. Geometrical dimensions of X-type LTPS models are the same as those in Section 2, and the element type is C3D8. The effect of element number on the calculation result has been examined. Finally, in total, 49,296 elements and 186,253 nodes have been meshed for X-type LTPS model, as shown in Figure 5. The symmetric

Figure 5: Finite element meshing.

boundary conditions were applied on the all around faces of the model, and the bottom surface of the lower face sheet was constrained. Similarly, a rigid plate was also added on the top surface of the upper face sheet in order to have a uniform deformation. A tensile load was applied on the rigid plate, and the displacement of the rigid plate was equal to the equivalent displacement of the X-type LTPS. The effective strain of the whole structure is also calculated by the displacement of rigid plate divided by the original total height of the LTPS. The obtained elastic stage of the equivalent stress-strain curve is also presented in Figure 4.

4 Results and discussion

4.1 Comparison between homogeneous method and FEM

Figure 4 shows the elastic stage of the stress-strain curve of the X-type LTPS obtained by homogeneous method and FEM. The two slopes by the two methods show a good agreement, indicating that the homogeneous method is right. The obtained EEM by the two methods are 393 MPa and 420 MPa, respectively, and the error is only 6.43%. It is a pity that we did not present an experimental validation, which still needs further study in the future.

4.2 Effect of the geometrical parameters

As shown in Figure 2, the X-type LTPS is determined by seven parameters including the thickness of face sheet T, stamping angle α , shearing angle β , truss length L, truss width w, truss thickness t and node length S. Basing on

the single-factor analysis, how these parameters affect the EEM is fully discussed here by the developed homogeneous method. When one of the parameters is discussed, its value is changed, and the rest of the parameters are kept constant. The initial values are listed in Table 1.

Figure 6 shows the effects of truss length, truss width, truss thickness, stamping angle, shearing angle, thickness of face sheet and node length on EEM by homogenization method. Obviously, as the truss length, stamping angle and shearing angle increase, the EEM decreases. The EEM decreases slightly as the node length increases, while it increases with the increase of truss width, truss thickness and thickness of face sheet. The effect of the geometrical parameters can be verified by previous work [30]. As the truss length increases from 14 to 22 mm, the EEM decreases from 1500 to 432 MPa. However, as the truss width and thickness increase from 1.5 to 3.5 mm and 1.0 to 1.8 mm, the EEM increases from 432 to 700 MPa and from 432 to 880 MPa, respectively. As the stamping and shearing angle increase from 10 to 70° and 20 to 60° , the EEM decreases from 1040 to 502 MPa and from 2024 to 494 MPa, respectively. And their decrease rates are 8.97 MPa and 38.25 MPa per each degree, respectively. As the thickness of face sheet increases from 1.2 to 3.2 mm, the EEM increases from 450 to 455 MPa slightly, while it decreases slightly from 620 to 460 MPa as the node length increases from 1 to 5 mm. As found above, the most significant important factors effecting the EEM are shearing angle, stamping angle, truss width, truss length and truss thickness, while the effects of the node length and face sheet thickness are not obvious.

4.3 Discussion of influence mechanism

To find out the reason why the geometric parameters have such significant effect on the EEM of X-type LTPS, we perform a stress analysis to a single truss as shown in Figure 7. P is a tensile load at the truss end in \overline{Z} direction. It is decomposed into three forces P_x , P_y and P_z in X, Y and Z directions, respectively, which produce axial tensile deformation D_x , bending deformation D_y and D_z in Y and Z directions, respectively.

 $P_{\rm y}$, $P_{\rm y}$ and $P_{\rm z}$ are calculated by

$$P_{X} = P\cos\frac{\alpha}{2}\cos\frac{\beta}{2}$$
 (16a)

$$P_{\rm Y} = P \sin \frac{\alpha}{2} \tag{16b}$$

$$P_{z} = P\cos\frac{\alpha}{2}\sin\frac{\beta}{2} \tag{16c}$$

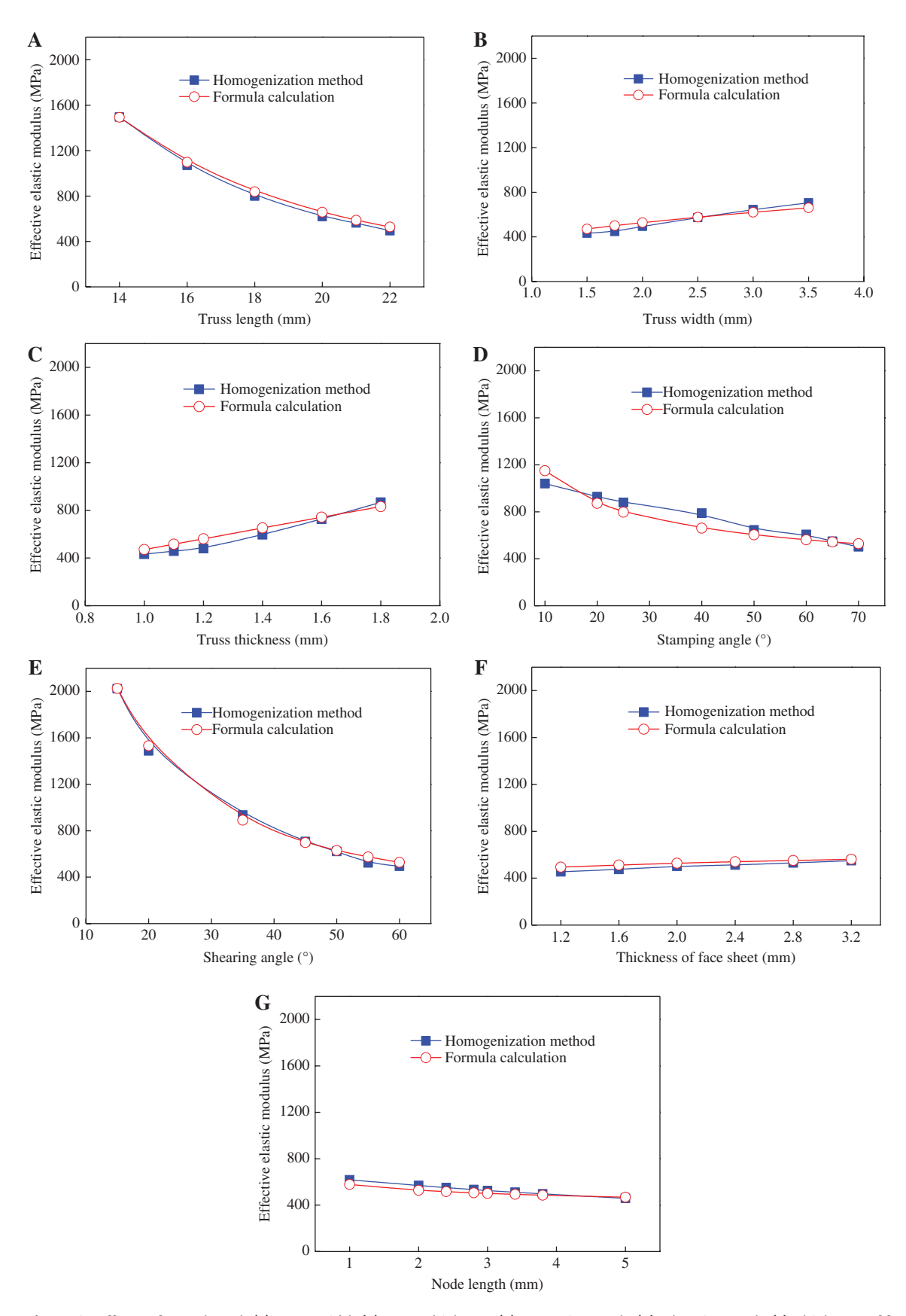


Figure 6: Effects of truss length (A), truss width (B), truss thickness (C), stamping angle (D), shearing angle (E), thickness of face sheet (F) and node length (G) on EEM.

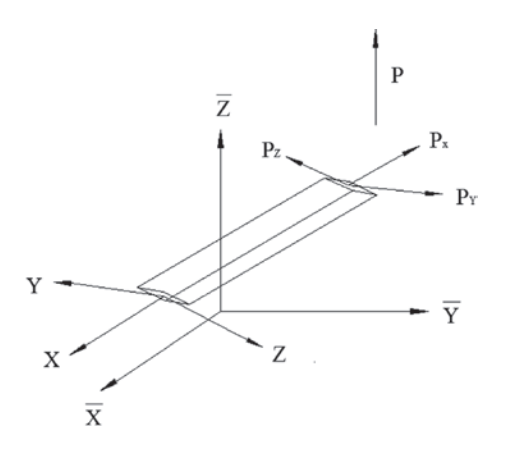


Figure 7: The force diagram of the beam.

 D_{x} , D_{y} and D_{z} are calculated by

$$D_{X} = \left(PL\cos\frac{\alpha}{2}\cos\frac{\beta}{2}\right)/EA \tag{17a}$$

$$D_{\rm Y} = P \sin \frac{\alpha}{2} L^3 / 3EI_{\rm Z} \tag{17b}$$

$$D_z = \left(P\cos\frac{\alpha}{2}\sin\frac{\beta}{2}L^3\right)/3EI_{\gamma}$$
 (17c)

where A is the cross-sectional area of truss, and I_{γ} and I_{Z} are the inertia moments of the cross-sectional area of truss about the Y and Z axes, respectively. We decompose D_{X} , D_{Y} and D_{Z} in \overline{Z} , directions, respectively:

$$d_{x} = \left(PL\cos^{2}\frac{\alpha}{2}\cos^{2}\frac{\beta}{2}\right)/EA \tag{18a}$$

$$d_{Y} = \left(P \sin^{2} \frac{\alpha}{2} \cos \frac{\beta}{2} L^{3}\right) / 3EI_{Z}$$
 (18b)

$$d_z = P\cos^2\frac{\alpha}{2}\sin^2\frac{\beta}{2}L^3/3EI_y \tag{18c}$$

 d_x , d_y and d_z are the deformation components induced by D_y , D_y and D_z in \overline{Z} direction.

The total displacement d' in \overline{Z} direction is the sum of d_x , d_y and d_z :

$$d' = d_X + d_Y + d_Z$$

$$= \frac{PL}{EA} \cos^2 \frac{\alpha}{2} \cos^2 \frac{\beta}{2} + \frac{PL^3}{3EI_Z} \sin^2 \frac{\alpha}{2} \cos \frac{\beta}{2}$$

$$+ \frac{PL^3}{3EI_Y} \cos^2 \frac{\alpha}{2} \sin^2 \frac{\beta}{2}$$
(19)

The truss height *H* shown in Figure 2 is calculated by

$$H = L\cos\frac{\alpha}{2}\cos\frac{\beta}{2} \tag{20}$$

The equivalent strain ε' in \overline{Z} direction is

$$\varepsilon' = \frac{d'}{H} = \left(P\cos\frac{\alpha}{2}\cos\frac{\beta}{2}\right) / Ewt + \left(4P\sin\frac{\alpha}{2}\tan\frac{\alpha}{2}L^2\right) / Ewt^3 + 4P\cos\frac{\alpha}{2}\sin\frac{\beta}{2}\tan\frac{\beta}{2}L^2 / Ew^3t$$
(21)

The EEM $(E_{\rho q})$ is calculated by

$$E_{eq} = \frac{\sigma}{\varepsilon'} \tag{22}$$

Having a derivation to L, w, t, α and β by Equation (21), respectively, we obtain

$$\frac{\partial \varepsilon'}{\partial L} = \left(8P\sin\frac{\alpha}{2}\tan\frac{\alpha}{2}L\right) / Ewt^3 + 8P\cos\frac{\alpha}{2}\sin\frac{\beta}{2}\tan\frac{\beta}{2}L / Ew^3t$$
(23)

$$\frac{\partial \varepsilon'}{\partial w} = -\left(P\cos\frac{\alpha}{2}\cos\frac{\beta}{2}\right) / Ew^2t - \left(4P\sin\frac{\alpha}{2}\tan\frac{\alpha}{2}L^2\right) / Ew^2t^3$$
$$-12P\cos\frac{\alpha}{2}\sin\frac{\beta}{2}\tan\frac{\beta}{2}L^2 / Ew^4t \tag{24}$$

$$\frac{\partial \varepsilon'}{\partial t} = -\left(P\cos\frac{\alpha}{2}\cos\frac{\beta}{2}\right) / Ewt^2 - \left(12P\sin\frac{\alpha}{2}\tan\frac{\alpha}{2}L^2\right) / Ewt^4$$
$$-4P\cos\frac{\alpha}{2}\sin\frac{\beta}{2}\tan\frac{\beta}{2}L^2 / Ew^3t^2$$
(25)

$$\frac{\partial \mathcal{E}'}{\partial \alpha} = -\left(P\sin\frac{\alpha}{2}\cos\frac{\beta}{2}\right)/2Ewt + (PL^2)/Ewt^3\cos\frac{\alpha}{2}$$

$$-2P\sin\frac{\alpha}{2}\sin\frac{\beta}{2}\tan\frac{\beta}{2}L^2/Ew^3t$$
(26)

$$\frac{\partial \mathcal{E}'}{\partial \beta} = -\left(P\cos\frac{\alpha}{2}\sin\frac{\beta}{2}\right)/2Ewt + P\cos\frac{\alpha}{2}L^2/Ew^3t\cos\frac{\beta}{2}$$
 (27)

After a calculation of Equations (23)–(27), it is found that $\frac{\partial \varepsilon'}{\partial L} > 0$, $\frac{\partial \varepsilon'}{\partial \alpha} > 0$, $\frac{\partial \varepsilon'}{\partial \beta} > 0$, which means that ε' increases with the increase of L, α and β (10° $\leq \alpha \leq$ 70°, 10° $\leq \beta \leq$ 60°). As a result, EEM decreases according to Equation (22), whist $\frac{\partial \varepsilon'}{\partial w} < 0$ and $\frac{\partial \varepsilon'}{\partial t} < 0$, which proves that the EEM increases as w and t increase.

The reason of node length *S* effect on EEM is discussed as follows:

As shown in Figure 2, the length $L_{\bar{x}}$ and width $L_{\bar{y}}$ of the unit cell are calculated, respectively, by

$$L_{\overline{x}} = 2L\sin\frac{\beta}{2} + 2w/\cos\frac{\beta}{2} \tag{28}$$

$$L_{\overline{y}} = 2L\sin\frac{\alpha}{2}\cos\frac{\beta}{2} + 2S - 2t \cdot \cos\frac{\alpha}{2}$$
 (29)

As the panel structure bears a distributed load p, the equivalent load P of each truss in \overline{Z} direction as shown in Figure 7 is calculated by

$$P = pL_{\overline{X}}L_{\overline{Y}}/4 = p\left(2L\sin\frac{\beta}{2} + 2w/\cos\frac{\beta}{2}\right)$$
$$\left(2L\sin\frac{\alpha}{2}\cos\frac{\beta}{2} + 2S - 2t\cdot\cos\frac{\alpha}{2}\right)/4 \tag{30}$$

Substituting Equation (30) into Equation (21), we obtain

$$\varepsilon' = \frac{d'}{H} = \left[p \left(2L\sin\frac{\beta}{2} + 2w/\cos\frac{\beta}{2} \right) \right]$$

$$\left(2L\sin\frac{\alpha}{2}\cos\frac{\beta}{2} + 2S - 2t \cdot \cos\frac{\alpha}{2} \right) / 4 \left[\left(\cos\frac{\alpha}{2}\cos\frac{\beta}{2} \right) / Ewt \right]$$

$$+ \left(4\sin\frac{\alpha}{2}\tan\frac{\alpha}{2}L^{2} \right) / Ewt^{3} + 4\cos\frac{\alpha}{2}\sin\frac{\beta}{2}\tan\frac{\beta}{2}L^{2} / Ew^{3}t \right]$$
(31)

in \bar{Z} direction decreases, which leads to a slight increase of EEM.

4.4 Formula fitted

Based on the above analysis, it shows that each parameter has a different effect on the EEM. It is essential to develop a theory formula to calculate the EEM by the seven variables. For foam materials, it has been proved that the EEM is related with the relative density $\bar{\rho}$ [23]:

$$E_{eq}/E \propto \overline{\rho}^n \quad (n > 0) \tag{33}$$

For low density foam, Equation (33) agrees well with experiment, but for large density foam they have no clear correlation [23].

In order to illustrate whether the LTPS obeys Equation (33), we plot the EEM as a function of relative density with different geometrical dimensions, as shown in Figure 8. It should be noted that when one parameter is discussed the other parameters are kept constant. Here the relative density of the X-type LTPS is calculated by

$$\overline{\rho} = \frac{wt \left(L + S/\cos\frac{\beta}{2} \right)}{\left(L\sin\frac{\beta}{2} + w/\cos\frac{\beta}{2} \right) \left(L \cdot \cos\frac{\beta}{2} \cdot \sin\frac{\alpha}{2} + S \cdot t \cdot \cot\left(45^{\circ} + \frac{\alpha}{4} \right) \right) \left(L \cdot \cos\frac{\beta}{2} \cdot \cos\frac{\alpha}{2} + t \right)}$$
(34)

Having a derivation to S by Equation (31), we obtain

$$\frac{\partial \mathcal{E}'}{\partial S} = p \left(L \sin \frac{\beta}{2} + w / \cos \frac{\beta}{2} \right) \times \left[\left(\cos \frac{\alpha}{2} \cos \frac{\beta}{2} \right) / Ewt + \left(4 \sin \frac{\alpha}{2} \tan \frac{\alpha}{2} L^2 \right) / Ewt^3 + 4 \cos \frac{\alpha}{2} \sin \frac{\beta}{2} \tan \frac{\beta}{2} L^2 / Ew^3 t \right]$$
(32)

It shows that $\frac{\partial \varepsilon'}{\partial S} > 0$, which proves that the ε' increases with the increase of S, and correspondingly the EEM decreases according to Equation (22).

As calculated in Section 2, it reveals that the effective modulus of lattice truss core is far smaller than that of face sheet. Therefore, the deformation of face sheet can be ignored compared with the core. As the thickness of face sheet increases, the total height of the panel structure increases, while the vertical deformation of core is constant at a constant stress. As a result, the effective strain

Figure 8 demonstrates that EEM of the X-type LTPS does not exhibit a clear correlation with the relative density. This conclusion is consistent with that of the pyramidal LTPS [30]. The EEM totally increases as the relative density increases. As the relative density is smaller than 2%, the effects of different parameters are similar. As the relative density is larger than 2%, the most significant impact factor is the shearing angle, and then followed by the truss width, length and thickness with the same effect; the smallest influencing factor is the stamping angle. Therefore, EEM cannot be simply expressed by a formula with relative density.

Gibson and Ashby [31] have developed a theoretical formula to calculate the EEM for honeycomb and foam structures which include the geometrical parameters of unit cells, respectively (see Equations (35) and (36)). Figures 9 and 10 show the sketching of the unit cells of honeycomb and foam structures, respectively. For honeycombs, there are four geometrical parameters including

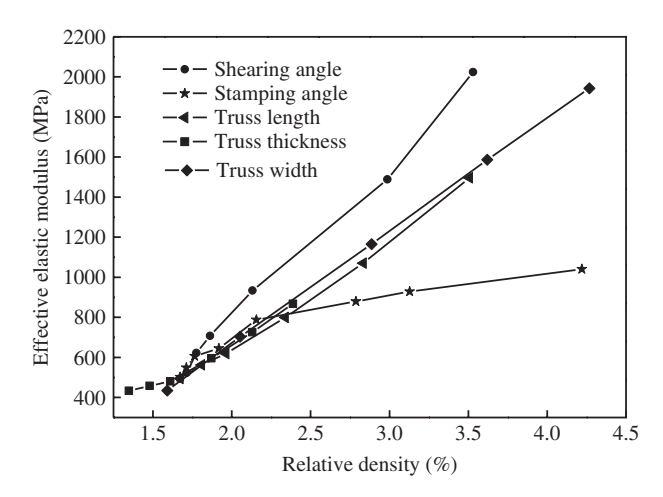


Figure 8: EEM of X-type LTPS versus relative density with different geometrical parameters.

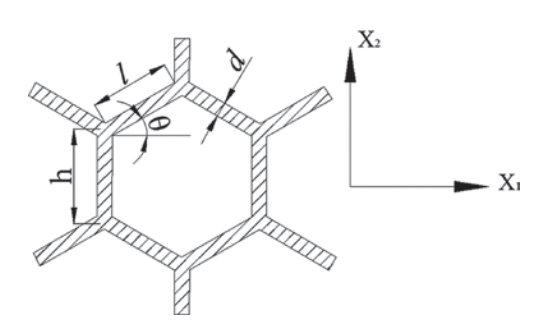


Figure 9: Unit cell of honeycomb structures.

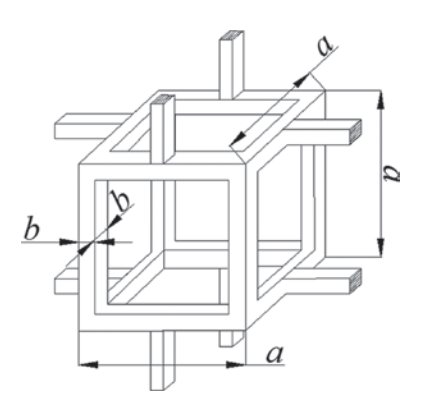


Figure 10: Unit cell of foams.

length of side l and h, wall thickness d and inclination angle of side θ . The foams have two geometrical parameters: length *a* and thickness *b*.

$$\frac{E_{eq}^{h}}{E_{o}} = \left\{ \frac{h/l + 2}{2(h/l + \sin\theta)\cos\theta} \right\} \frac{d}{l} = \overline{\rho} \approx \frac{d}{l}$$
 (35)

$$\frac{E_{eq}^f}{E_o} = \frac{C_1 I}{a^4} = C_1 \overline{\rho}^2 \tag{36}$$

where E_{eq}^h and E_{eq}^f denote the EEM of honeycomb and foam structures, respectively. E_0 is the Young's modulus of the parent material. $\overline{\rho}$ is the relative density. C_1 and I are the constant of proportionality and the second moment of

However, the honeycomb structures belong to the ordered two-dimensional cellular solid, and foams belong to unordered cellular solid, whereas X-type LTPS belongs to ordered three-dimensional cellular solid. Besides, the honeycomb and the foam structures include four and two geometrical parameters, respectively, while the X-type LTPS has seven geometrical parameters. The EEM proposed by Gibson and Ashby is not suitable for X-type LTPS. Therefore, it is essential to establish the relationship between the EEM and geometrical parameters of X-type LTPS. The structure of LTPS is very complex, and it is very difficult to get an analytical formula to calculate the EEM. In order to get a formula, we performed a large number of FEM calculations with different geometric dimensions and then fitted a formula by Origin software as follows

$$E_{eq} = E_0 \left[\left(\frac{t}{\beta} \right)^{0.97} \left(\frac{w}{\alpha} \right)^{0.41} \left(\frac{T}{S} \right)^{0.13} \frac{700}{L^{2.30}} \right]$$
 (37)

where E_{eq} is the EEM, and E_0 is the elastic modulus of basic metal. Their unit is megapascal. The units of the geometrical parameters L, w, t, T, and S are millimeters, and the units of α , β are degrees. But only the values of the geometrical parameters are put into Equation (37), and their units are not considered in the calculation.

The EEM of the X-type LTPS with different geometrical parameters derived from the present fitted formula Equation (37) is also plotted in Figure 6. It obviously shows that there is a good consistence between the homogenization and formula results, which proves that the present formula can be used to calculate the EEM. Kawashima et al. [32] and Mizokami et al. [33] studied the effective strength of plate-fin structure. The porous structure is treated as the equivalent homogenous solid plate, and the tensile and creep strength are predicted successfully. In their method, the calculation of EEM is an important issue, and they predict it by FEM. But how the geometrical parameters influence the EEM is still unclear. The effective mechanical strength of LTPS, such as tensile, creep and fatigue, still needs to be studied further by the equivalent homogenous solid method, and the formula can be used to calculate the EEM for future work, proving that this work plays a key role for the development of structural design procedure of compact heat exchanger by LTPS. It should be noted that the flexural deformation has not been considered in this

model [8], because for heat exchanger it is forbidden to have such obvious deformation in order to ensure safety. The effect of flexural deformation on strength still needs further study in the future.

5 Conclusions

In this study, the EEM of X-type LTPS has been investigated by homogenization method and FEM; meanwhile, the effects of the seven geometric parameters on the EEM of X-type LTPS are explored. Based on this study, the following conclusions can be drawn.

- The results by homogenization method and FEM have a good agreement, which proves that the homogenization method is right.
- With the increase of stamping angle, shearing angle, truss length, and node length, the EEM of X-type LTPS decreases. With the increase of truss width, truss thickness and thickness of face sheet, the EEM increases.
- The EEM does not exhibit a clear correlawith the relative density. The formula, 700 S $I^{2.30}$ can be used to accurately calculate the EEM.

Acknowledgments: The authors gratefully acknowledge the support provided by the Construction Project of Taishan Scholars (ts201511018), the Natural Science Foundation for Distinguished Young Scholars of Shandong Province (JQ201417), National Natural Science Foundation of China (11372359) and the Fundamental Research Funds for the Central Universities (15CX08006A).

References

- [1] Fan HL, Jin FN, Fang DN. Mater. Des. 2009, 30, 511-517.
- [2] Lu TJ, Valdevit I, Evans AG. Prog. Mater. Sci. 2005, 50, 789-815.
- [3] Queheillalt DT, Carbajal G, Peterson GP, Wadley HNG. Int. J. Heat Mass Transf. 2008, 51, 312-326.
- [4] El-Magd E, Gebhard J, Stuhrmann J. Comp. Mater. Sci. 2007, 39, 446-452.

- [5] Hu Y, Li W, An X, Fan H. Compos. Sci. Technol. 2016, 125,
- [6] Tan Z, Bai L, Bai B, Zhao B, Li Z, Hou H. Mater. Des. 2016, 92, 724-730.
- [7] Queheillalt DT, Murty Y, Wadley HNG. Scr. Mater. 2008, 58, 76-79.
- [8] Chen H, Zheng Q, Zhao L, Zhang Y, Fan H. Compos. Struct. 2012, 94, 3448-3456.
- [9] Zhang Y, Xue Z, Chen L, Fang D. Int. J. Mech. Sci. 2009, 51, 213-221.
- [10] Dong L, Deshpande V, Wadley H. Int. J. Solids Struct. 2015, 15, 107-124.
- [11] Liu X, Liang N. J. Mech. Phys. Solids 2012, 60, 1722–1739.
- [12] Gibson LJ. Mater. Sci. Eng. A 1989, 110, 1–36.
- [13] Torquato S, Gibiansky LV, Silva MJ, Gibson LJ. Int. J. Mech. Sci. 1998, 40, 71-82.
- [14] Wallach JC, Gibson LJ. Int. J. Solids Struct. 2001, 38, 7181-7196.
- [15] Sanders WS, Gibson LJ. Mater. Sci. Eng. A 2003, 347, 70–85.
- [16] Sanders WS, Gibson LJ. Mater. Sci. Eng. A 2003, 352, 150-161.
- [17] Guessasma S, P Babin, Della Valle G, Dendievel R. Int. J. Solids. Struct. 2008, 45, 2881-2896.
- [18] Guessasma S. Comput. Mater. Sci. 2008, 44, 552-565.
- [19] Antunes FV, Ferreira JAM, Capela C. Finite Elem. Anal. Des. 2011, 47, 78-84.
- [20] Marur PR. Finite Elem. Anal. Des. 2010, 46, 1001-1007.
- [21] Pérez L, Lascano S, Aguilar C, Estay D, Messner U, Figueroa IA, Alfonso I. Comput. Mater. Sci. 2015, 110, 281-286.
- [22] Pérez L, Lascano S, Aguilar C, Domancic D, Alfonso I. Mater. Des. 2015, 83, 276-283.
- [23] Liu R, Antoniou A. Acta Mater. 2013, 61, 2390-2402.
- [24] Chen Z, Wang X, Giuliani F, Atkinson A. Acta Mater. 2015, 89,
- [25] Ohno N, Ikenoya K, Okumura D, Matsuda T. Int. J. Solids Struct. 2012, 49, 2799-2806.
- [26] Liu T, Deng ZC, Lu TJ. Int. J. Solids Struct. 2007, 44, 3231-3266.
- [27] Liu T, Deng ZC, Lu TJ. Int. J. Solids Struct. 2006, 43, 7891-7918.
- [28] Zhang QC, Chen AP, Chen C. Sci. China Ser. E-Tech. Sci. 2009, 52, 2147-2157.
- [29] Zhang Q, Chen A, Chen C, Lu T. Sci. China Ser. E 2009, 7, 1216-1227.
- [30] Zhang Q, Jiang W, Zhao B, Luo Y, Tu ST. Compos. Struct. 2017, 165, 130-137.
- [31] Gibson LJ, Ashby MF. Cellular Solids: Structure and Properties, Cambridge University Press: Cambridge, 1999, Vol. 11, pp 655-656.
- [32] Kawashima F, Igari T, Miyoshi Y, Kamito Y, Tanihira M. Nucl. Eng. Des. 2007, 237, 591-599.
- [33] Mizokami Y, Igari T, Kawashima F, Sakakibara N, Tanihira M, Yuhara T, Hiroe T. Nucl. Eng. Des. 2013, 255, 248-262.